NUMERICAL MODELLING OF MICROWAVE HEATING OF FROZEN WOOD

F. Erchiqui,[1]* Z. Annasabi,[1] A. Koubaa,[1] F. Slaoui-Hasnaoui[1] and H. Kaddami[2]

1. Department of Applied Sciences, University of Québec at Abitibi-Témiscamingue, Rouyn-Noranda, Quebec, Canada J9X 5E4

2. Université Cadi Ayyad, Marrakech, Morocco

The heating process of frozen wood exposed to plane microwaves is numerically investigated. The nonlinear heat conduction problem involving phase change such as wood freezing is solved by a specific 3D volumetric enthalpy-based finite element method. Dielectric and thermal properties are a function of temperature and moisture content. The numerical model is validated by experimental and analytical means. As an application, we studied the effect of moisture content and frequency on microwave heating of trembling aspen wood.

Keywords: Beer–Lambert's law, frozen wood, microwave heating, trembling aspen

INTRODUCTION

Industrial microwave heating came into use after the Second World War.[1] In fact, the research on high-resolution radar during that war led to the development of microwave frequencies, principally with magnetron of microwaves generator.[1] Further development resulted in the use of microwaves for domestic and industrial heating. The advantages of microwave over lower-frequency treatments have led to a number of applications in areas such as food industries,[2] chemical industries,[3] and medical fields.[4] For industrial applications, microwave heating is generally performed at frequencies between 900 and 2450 MHz.[1] Microwave irradiation is a method of heating less conductive (dielectric) materials electrically and, generally, thermally. Unlike infrared heating, which requires an outer surface, dielectric heating allows heat to be produced within the material and in a shorter time.

In microwave heating, the microwave's electric field polarises the dipole molecules contained in the material.[5] Depending on the frequency, the dipole molecules may rotate in continuous alignment with the electric field. If the dipoles lag behind the electric field, then interactions between the dipole and the electric field lead to energy loss within the material as the material heats.[5] The quantity of energy lost over time depends on the phase difference between the applied electric field and the dipole moment of the molecules as well as the mobility of the electron clouds within the molecules present in the material.

In wood, the water content is either bound or free. Bound water is held within the cell walls by bonding forces between water and cellulose molecules. Free water is contained in the cell cavities and is not held by these forces; it is comparable to water in a pipe. The amount of power dissipated depends on the extent of the hydrogen-bonded network. An applied electric field induces asymmetry of the water molecules (polarisation) present in the material. Consequently, at particular frequencies, the molecules become agitated and generate heat in the material. In free liquid water, this agitation occurs at GHz frequencies (microwaves), whereas in more restricted bound water it occurs at MHz frequencies (short radiowaves), and in ice it occurs at kHz (long radiowaves).[1]

Microwave heating of frozen wood is a complex process that exhibits highly nonlinear interactions among the mechanical, thermal and electrical properties. This poses a daunting challenge for numerical simulation, because the combined complexities of heat and mass transfer, phase change, and thermomechanical and electromagnetic interaction must be considered.[6–18] However, in the literature on microwave heating process, three numerical methods are used to solve the equations describing this process (finite differences, finite control volume and finite elements) and the absorbed power per unit volume is generally modelled based on Lambert's Law. In this regard, in Ref.[11] the authors have studied one-dimensional heating and solved heat transfer equations in a meat block heated by microwaves. Swami[12] has used a finite difference model to describe heating of gels with high water and NaCl content. Steinhagen and Harry[13] have used the one-dimensional explicit finite-difference method. For this, the enthalpy formulation is used to compute transient temperatures of logs. Ratanadecho[8] has used a finite control volume discretisation method to simulate the heating of liquid layers using a rectangular wave guide and analysed the influence of frequency and the size of the samples.

However, the finite element method is largely used to solve differential equations for microwave heating. The authors in Ref.[14] have employed finite elements with the Galerkin formulation for predicting potato heating in cylindrical geometry. Zhou et al.[15] have developed a three-dimensional finite element model to predict temperature within foods heated by microwaves. Ayappa et al.[16] have developed a general formulation for microwave power absorbed by a homogeneous isotropic multilayered medium and analysed the temperature profile within multilayered foods exposed to planes waves. In Ref.,[17] the authors solved a model taking into account energy and mass transfer during heating. Datta and Anantheswaran[18] have included recent developments in modelling of microwave heating process to predict temperature within foods heated by microwaves.

However, when the medium undergoes a phase change (example: solid to liquid), the numerical solution is more difficult because of the presence of one or more moving borders for

*Author to whom correspondence may be addressed.
E-mail address: fouad.erchiqui@uqat.ca
Can. J. Chem. Eng. 91:1582–1589, 2013

DOI 10.1002/cjce.21826
Published online 26 April 2013 in Wiley Online Library (wileyonlinelibrary.com).

solid–liquid phases. In general, for this type of problem, there are two approaches to solve this problem: solve separately the equations of energy for liquid and solid phases, taking into account the moving boundary (solid–liquid interface) or solve the equation of energy in term of the enthalpy function. However, we believe that using a solution in terms of enthalpy is more appropriate where there is the phase changing phenomena. The enthalpy function is a physical function that is well defined for both solids and liquids. The advantage of using an enthalpy rather than a temperature-based formulation is that it simultaneously eliminates the doubling of the energy equation. By introducing the volumetric specific enthalpy $H(T)$ at the phase transition, the abrupt jump in the volumetric heat capacity is transformed into a relatively smoother temperature-dependent function. It can be shown that around the phase transition the curvature of volumetric specific enthalpy $H(T)$ is similar to that of thermal conductivity $k(T)$.

In this study, the heating process of frozen wood exposed to plane microwaves is numerically investigated. For this, the nonlinear heat conduction problem involving phase change is solved by a specific 3D volumetric enthalpy-based finite element method. The dielectric and thermal properties of the wood are considered as functions of temperature and moisture content. The wood medium is assumed linear for electromagnetic wave propagation. We used the Maxwell results to solve the nonlinear heat conduction problem involving phase changes, such as the freezing of wood, using a 3D enthalpy-based finite element method. The numerical simulations of the proposed approach (*volumetric enthalpy-method*) have allowed validating the analytical and experimental results. As an application, we studied the effect of moisture content and frequency on microwave heating of trembling aspen wood.

ENTHALPY MODEL FOR HEATING

In this study, we assume that the interface Γ between the solid (Ω^-) and liquid (Ω^+) phases can be described by a regular function $F(x, y, z, t) = 0$.[19] The temperature in the solid and liquid phases is denoted by T_s and T_l respectively. Using a temperature-based formulation, the two energy equations that govern both solid and liquid media are written in the absence of convective motion:

$$\rho^s(T_s)C_p^s(T_s)\frac{\partial T_s}{\partial t} = \nabla\cdot(k^s(T_s)\nabla T_s), \quad F(x,y,z) < 0 \tag{1a}$$

$$\rho^l(T_l)C_p^l(T_l)\frac{\partial T_l}{\partial t} = \nabla\cdot(k^l(T_l)\nabla T_l), \quad F(x,y,z) > 0 \tag{1b}$$

where ρ^s [kg/m^3], C_p^s [J/kg/°C] and k^s [W/m/°C] are respectively the density, the specific heat capacity and the thermal conductivity of the material in the solid state. ρ^l [kg/m^3], C_p^l [J/kg/°C] and k^l [W/m/°C] are respectively the density, the specific heat capacity and the thermal conductivity of the material in the liquid state. The boundary conditions, also known as the Stefan conditions,[19] allow considering the energy jump between the two phases:

$$T_s(x,y,z,t) = T_l(x,y,z,t); \quad F(x,y,z,t) = 0 \tag{2a}$$

$$k^s(T_s)\nabla T_s\cdot\nabla F - k^l(T_l)\nabla T_l\cdot\nabla F = -\rho\cdot L\frac{\partial F}{\partial t}, \quad F(x,y,z,t) = 0 \tag{2b}$$

L is the latent heat [J/kg]. In order to avoid numerical problems in the phase transition region, the variables were changed. The temperature-dependent density $\rho(T)$ and specific heat capacity $C_p(T)$ can be replaced by the volumetric specific enthalpy $H(T)$ defined by[20]:

$$H(T) = \int_{T_{ref}}^{T}\rho(T)C_p(T)\mathrm{d}T \tag{3}$$

where T_{ref} [°C] is a reference temperature. The advantage of using an enthalpy- rather than a temperature-based formulation is that it simultaneously eliminates the doubling of the energy equation and the Stefan conditions. By introducing the volumetric specific enthalpy $H(T)$ at the phase transition, the abrupt jump in the volumetric heat capacity is transformed into a relatively smoother temperature-dependent function. It can be shown that around the phase transition the curvature of volumetric specific enthalpy $H(T)$ is similar to that of thermal conductivity $k(T)$. $H(T)$ depends strongly on the type of material, but we must distinguish between two distinct situations. In the first case, the phase change occurs in an interval $[T_1^s - T_2^f]$. In this case the enthalpy is defined by:

$$H(T \le T_1^s) = \int_{T_{ref}}^{T}\rho^s(T)C_p^s(T)\mathrm{d}T \tag{4a}$$

$$H(T_1^s \le T \le T_2^f) = \int_{T_{ref}}^{T_1^s}\rho^s(T)C_p^s(T)\mathrm{d}T + \int_{T_1^s}^{T}\rho(T)\frac{\partial L}{\partial T}\mathrm{d}T \tag{4b}$$

$$H(T > T_2^f) = \int_{T_{ref}}^{T_1^s}\rho^s(T)C_p^s(T)\mathrm{d}T + \rho(T)L + \int_{T_2^f}^{T}\rho^f(T)C_p^f(T)\mathrm{d}T \tag{4c}$$

In the second case, the phase change occurs at a constant temperature, so the enthalpy exhibits discontinuity at the temperature fusion $T_m(= T_1^s = T_2^f)$, and is defined as follows:

$$H(T \le T_m) = \int_{T_{ref}}^{T}\rho^s(T)C_p^s(T)\mathrm{d}T \tag{5a}$$

$$H(T > T_m) = \int_{T_{ref}}^{T_1^s}\rho^s(T)C_p^s(T)\mathrm{d}T + \rho(T)L + \int_{T_m}^{T}\rho^f(T)C_p^f(T)\mathrm{d}T \tag{5b}$$

Zero enthalpy is defined at the saturated solid temperature. For purposes of numerical simulation, the enthalpy method is more reliable. However, the problem remains difficult and highly nonlinear. Following a procedure similar to the enthalpy transform method, the temperature-dependent thermal conductivity $k(T)$ can be substituted with the thermal conductivity integral θ, using Kirchhoff's transformation:

$$\theta(T) = \int_{T_{ref}}^{T}k(T)\mathrm{d}T; \quad \forall T \tag{6}$$

By using the Leibniz's rule[21] for differentiation under the integral sign in Equation (6), the governing heat equation reduces to a partial differential system, with two mutually related dependent

variables H and θ:

$$\frac{\partial H(T)}{\partial T} = \nabla^2\theta(T) + Q_{\text{wave}} \tag{7}$$

where Q_{wave} is the power dissipated per unit volume (due to the microwave heating source). Combining the enthalpy transform and Kirchhoff's transform, six relationships between the variables H, θ and T are determined: $H(T)$, $\theta(T)$, $T(H)$, $T(\theta)$, $H(\theta)$ and $\theta(H)$. All these functions are supposed increase monotonically and continuously because $\rho(T)$, $C_{\text{p}}(T)$ and $k(T)$ are positive and bounded.[22] Consequently, a one-to-one mapping exists between the independent and dependent variables in the Equation (7). This equation is valid for both phases, where all the thermal properties now vary with temperature. In this way, the nonlinearities originating from the temperature-dependent thermo-physical material properties are removed from the governing equation and incorporated into a functional relationship between the volumetric specific enthalpy and the Kirchhoff function. By introducing this functional relationship, the curvature of $\rho(T)$, $C_{\text{p}}(T)$ and $k(T)$ around the phase transition become less problematic and the numerical integration process is simplified. Finally, the radiative source term is given by the following formula (see the Modelling Microwave Heating Section):

$$Q_{\text{wave}} = -\text{Re}\{\nabla \cdot \boldsymbol{S}\} \tag{8}$$

where $\boldsymbol{S}$ is the Poynting vector and Re denotes the real part of a complex number. The vector $\boldsymbol{S}$ describes the radiative flux density associated with the propagation of electromagnetic waves and the energy dissipated in the material medium:

$$\boldsymbol{S} = \frac{1}{2}\boldsymbol{E} \times \boldsymbol{H}^* \tag{9}$$

$\boldsymbol{E}$ and $\boldsymbol{H}^*$ are respectively the electric field and the conjugate of the magnetic field $\boldsymbol{H}$. In this work we consider that the heat is isotropic. To solve the problem, we introduce into Equation (7) the boundary condition, as follows:

$$\nabla\theta \cdot \mathbf{n} + h(T - T_\infty) - \mathbf{q} \cdot \mathbf{n} = 0 \tag{10}$$

where $\mathbf{q}$ is the radiative heat flux incident, $\mathbf{n}$ is the outward normal to the surface, h is the surface heat transfer coefficient [W/m^2/$^\circ$C] and T_∞ is the temperature of the surrounding medium (air). The term $h\ (T - T_\infty)$ represents the convection heat transfer from the material to the environment. The incident heat flux depends on the source configuration and the position of the material.

Finite Element Formulation

Space approximation

Galerkin's finite element method is widely used for modelling heat transfer. Regardless of the spatial dimensionality of the heat problem, the finite element method leads to first-order equations of a rank equal to the total number of nodes on the geometric mesh.

Assuming that the enthalpy H is defined uniquely in terms of the temperature T, we can express the Kirchhoff transform θ as a function of H. We then derive the following algebraic system:

$$C \cdot \frac{\partial H}{\partial t} + \bar{K} \cdot H + G \cdot H^2 = R + Q \tag{11}$$

where C is the global matrix of heat capacity, $\bar{K}$ and G are matrices of thermal conductance, and $(R + Q)$ is the nodal thermal load vector. To improve the numerical stability of (11), the capacitance matrix C is diagonalised (lumped). Although lumping introduces numerical diffusion, it eliminates undesirable oscillations generated by consistent (unlumped) mass matrices.

Implicit time integration scheme

Numerical time approximation schemes are used mainly to obtain the transient response. These numerical integration schemes derive recursion relations that relate $H(t)$ at a moment of time t to $H(t + \Delta t)$ at another moment of time $t + \Delta t$. The solution is then solved step by step starting from the initial conditions at time $t = 0$ until the desired duration of the transient response is calculated. The most common numerical schemes for the solution of Equation (11) belong to the weighted Euler difference family of time approximations, as follows:

$$H^{\mathbf{n}+\theta} = (1 - \theta)H^{\mathbf{n}} + \theta H^{\mathbf{n}+1}, \text{ with } \quad \theta = \frac{t - t_n}{\Delta t} \tag{12}$$

The parameter θ varies in the range [0–1]. The θ schemes are unconditionally stable when $\theta \geq 1/2$ and $O(\Delta t)$ are accurate, with the exception of the $O(\Delta t^2)$—convergent Crank–Nicolson scheme ($\theta = 1/2$). Setting $\theta = 1$ leads to the backward Euler (fully implicit) scheme, which is only first-order accurate, but very stable and hence ideally suited for integration. In the present study, we consistently use the implicit Crank–Nicolson scheme.[23] In this case, Equation (11) becomes:

$$(\hat{\boldsymbol{K}}_{n+1} + \hat{\boldsymbol{G}}_{n+1}) \cdot \boldsymbol{H}_{n+1} = \widehat{K}_n \cdot \boldsymbol{H}_n + \hat{\boldsymbol{G}}_n \cdot \boldsymbol{H}_n^2 + \hat{\boldsymbol{R}}_{n,n+1} \tag{13}$$

where $\hat{\boldsymbol{K}}, \hat{\boldsymbol{G}}$ and $\hat{\boldsymbol{R}}$ are modified global matrices and $\boldsymbol{H}_{n+1}$ is the vector of global nodal enthalpies at moment t_{n+1}.

Modelling Microwave Heating

A propagating electromagnetic wave is composed of oscillating electric ($\boldsymbol{E}$) and magnetic ($\boldsymbol{H}$) fields. The space and time dependence of these fields are described by the following Maxwell's equations[7]:

$$\nabla \times \boldsymbol{E} = -\frac{\partial \boldsymbol{B}}{\partial t} \tag{14}$$

$$\nabla \times \boldsymbol{H} = \boldsymbol{J} + \frac{\partial \boldsymbol{D}}{\partial t} \tag{15}$$

where $\boldsymbol{E}$, $\boldsymbol{D}$, $\boldsymbol{B}$, $\boldsymbol{H}$ and J are respectively the electric field (V/m), the electric displacement (Coulomb/m/m), the magnetic field (Weber/m), the magnetic induction (Weber/m) and the current density (A/m/m). In this work, we are interested in the radiation response of a particular frequency ω (rad/s). Thus, we consider the alternating field:

$$\boldsymbol{E}(x, y, z, t) = \bar{\boldsymbol{E}} \exp(j\,\omega\, t) \tag{16}$$

$$\boldsymbol{H}(x, y, z, t) = \bar{\boldsymbol{H}} \exp(j\,\omega\, t) \tag{17}$$

where $\bar{E}$ and $\bar{H}$ are real functions of (x, y and z) but not of time. In the case of linear material to which Ohm's law applies, we have the following relations:

$$\boldsymbol{J}(t) = \sigma(\omega)\boldsymbol{E}(t),\ \boldsymbol{D}(t) = \varepsilon(\omega)\boldsymbol{E}(t),\ \boldsymbol{B}(t) = \mu\ (\omega)\boldsymbol{H}(t) \tag{18}$$

where $\sigma(\omega)$, $\varepsilon(\omega)$ and $\mu(\omega)$ are respectively the conductivity, the dielectric constant and the magnetic permeability. These electrical properties are generally complex functions of the microwave radiation frequency ω. In wood material, the relation $\mu\ (\omega) = \mu_0$ is generally considered (μ_0 is the permeability of free space). With this assumption, the electroneutrality of wood ($\nabla(\nabla \cdot \boldsymbol{E}) = 0$), and using the relation $\nabla \times \nabla \times \bar{E} = \nabla(\nabla \cdot \bar{E}) - \nabla^2\bar{E}$, we deduce by substituting (16) and (17) in (14) and (15) the expression of Helmholtz's equation of wave propagation:

$$\nabla^2\bar{\boldsymbol{E}} + k_\omega^2\bar{\boldsymbol{E}} = 0 \tag{19}$$

for which we have:

$$k_\omega = \alpha_\omega + j\beta_\omega \tag{20}$$

k_ω is the propagation constant of the microwave radiation at frequency ω. α_ω and β_ω are related to the dielectric properties of the medium and the microwave radiation frequency by the following formulae:

$$\alpha_\omega = \frac{2\pi f}{c}\sqrt{\frac{\kappa'_\omega\left(\sqrt{1+\tan^2\delta_\omega} - 1\right)}{2}} \tag{21a}$$

$$\beta_\omega = \frac{2\pi f}{c}\sqrt{\frac{\kappa'_\omega\left(\sqrt{1+\tan^2\delta_\omega} + 1\right)}{2}} \tag{21b}$$

κ'_ω is the relative dielectric constant, κ''_ω the relative dielectric loss and δ_ω is the dielectric loss angle[11]:

$$\kappa'_\omega = \frac{\varepsilon(\omega)}{\varepsilon_0} = \frac{\varepsilon'(\omega)}{\varepsilon_0},\quad \kappa''_\omega = \frac{\sigma(\omega)}{\varepsilon_0\omega} = \frac{\varepsilon''(\omega)}{\varepsilon_0}\quad \text{and}\quad \tan(\delta_\omega) = \frac{\kappa''_\omega}{\kappa'_\omega} \tag{22}$$

where ε_0 is the permittivity of free space, ε' represents the material's ability to store electrical energy (characterised by direct measurement of the material's polarisation), and ε'' is the energy loss through dissipation in the dielectric material. In Equations (21a) and (21b) we used the property $c = 1/\sqrt{\mu_0\ \varepsilon_0}$ (where c is the velocity of light) and replaced ω by $2\pi f$, where f is the microwave radiation frequency.

Thus, if z denotes the propagation direction of the electromagnetic wave in the material, the following electric field is a useful solution to Helmholtz's Equation (19):

$$\bar{\boldsymbol{E}} = \boldsymbol{E}_0(x, y, z)\exp(-\alpha_\omega z)\exp(-j\beta_\omega z) \tag{23}$$

where the arbitrary amplitude factor $\bar{\boldsymbol{E}}$ may be replaced by $\boldsymbol{E}_0$ at $z = 0$ and $t = 0$. Equation (23) implies that the electrical field $\bar{\boldsymbol{E}}$ within the material will decay exponentially with distance from the surface. At higher frequencies, α_ω increases and the microwave penetration into the material decreases. $1/\alpha_\omega$ is the characteristic penetration depth, that is the distance at which the field intensity decreases to $1/e$ of the incident value. β_ω is the phase factor (this factor represents the change phase of the propagating wave).

Power Dissipation and Poynting's Theorem

The power flux associated with microwave propagation is represented by the Poynting vector **S** and time-averaged flux for harmonic fields. It is expression is given by Equation (9). The Poynting theorem allows the evaluation of the microwave power input. It is expressed as:

$$\nabla \cdot \boldsymbol{S} = -\frac{1}{2}\omega_0\varepsilon_0\kappa''_\omega\boldsymbol{E}\cdot\boldsymbol{E}^* + j\omega\left(\frac{\mu_0}{2}\boldsymbol{H}\cdot\boldsymbol{H}^* + \frac{\varepsilon_0\kappa'_\omega}{2}\boldsymbol{E}\cdot\boldsymbol{E}^*\right) \tag{24}$$

Considering the real part of (24), we obtain:

$$Q_{\text{wave}} = -\text{Re}\{\nabla \cdot \boldsymbol{S}\} = \frac{1}{2}\omega_0\varepsilon_0\kappa''_\omega|\boldsymbol{E}|^2 \tag{25}$$

Hence, with knowledge of the electrical field intensity in the medium, the local power dissipated is obtained from Equation (25). In the case where the propagation of uniform plane wave in a semi-infinite medium, the expression of the power dissipated per unit volume is given by:

$$Q_{\text{wave}} = \frac{1}{2}\omega_0\varepsilon''_\omega|\tau_\omega E_0|^2\exp(-2\alpha_\omega z) \tag{26}$$

where the term $(2/\alpha_\omega)$ is the penetration depth. This term is even smaller when the material is suitable for dielectric heating. We note an exponential decay of power. In practice, this result is approximately acceptable for the microwave treatment of wood and food. This is because most wood and foods have a relatively high effective loss factor ε''_ω, resulting in a rapidly decaying electric field, which justifies the above assumption.

NUMERICAL VALIDATION

The dynamic finite element method outlined in the previous section was implemented in the general purpose finite element code ThermoForm, developed by the principal author. All computations were performed in single precision on a PC.

Analytical Heating Validation

To validate the enthalpy approach we used to describe microwave heating, we consider the Beer–Lambert equation and a semi-infinite aluminium sample. The sample is exposed to microwave radiation on the left face. The initial sample temperature is 10°C and the heating time is 3000 s. For the analytical solution, we consider a semi-infinite medium[24] subjected to a uniform incident flux. The thickness and the physical properties of the material used for the numerical validation are given in Table 1.

The temperature $T(z,t)$ across the thickness with time t is computed using Laplace's transforms in order to solve the 1D energy equation with a source per unit volume. The boundaries of this medium are considered adiabatic. The analytical solution is given

Table 1. Geometrical and thermo-physical properties

Density, ρ (kg/m^3)	2702
Thermal conductivity, k (W/m/°C)	237
Specific heat, C_p (J/kg/°C)	903
Absorption coefficient, A (m^{-1})	10
Thickness, h_0 (m)	2
Heat flux, q'_0 (W/m^2)	1000

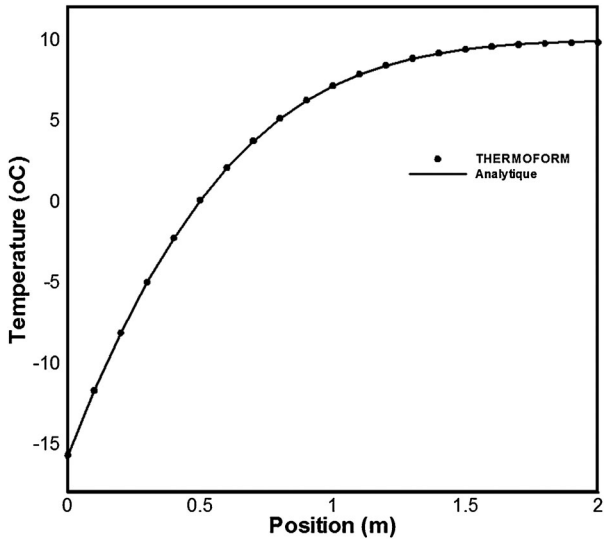

Figure 1. Temperature distribution at $t = 3000$ s.

by the following equation[24]:

$$T = T_{\text{init}} - \frac{q_0' e^{-Az}}{kA} + 2\frac{q_0'}{k}\sqrt{\alpha t}\,\text{ierfc}\left(\frac{z}{2\sqrt{\alpha t}}\right) + \frac{q_0'}{2kA}e^{A^2\alpha t + Az}\text{erfc}\left(A\sqrt{\alpha t} + \frac{z}{2\sqrt{\alpha t}}\right) + \frac{q_0'}{2kA}e^{A^2\alpha t - Az}\text{erfc}\left(A\sqrt{\alpha t} - \frac{z}{2\sqrt{\alpha t}}\right) \quad (27)$$

Figures 1 and 2 compare the predicted temperature obtained by the theoretical equation with the ThermoForm results. The results show excellent agreement between the theoretical and numerical solutions, with less than 0.1% discrepancy.

Experimental Heating Validation

To validate the enthalpy approach with experimental data, we consider experimental temperature measurements obtained by heating a frozen wood sample.[13] The thermo-physical properties of the material are given below:

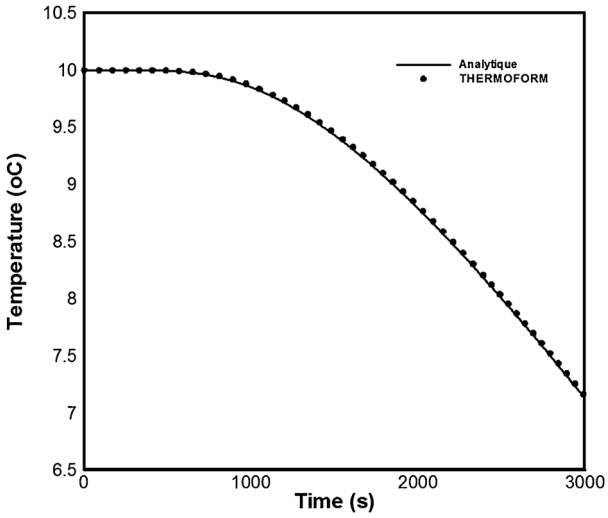

Figure 2. Change in temperature at the centre of the sample.

Density

Density is calculated as[25]:

$$\rho = 1000 G_{\text{m}}\left(1 + \frac{\text{MC}}{100}\right); \quad (\text{kg/m}^3) \quad (28)$$

MC is the moisture content in % and G_{m} is the specific gravity based on volume at the moisture content of interest.

Thermal conductivity

Thermal conductivity in the radial direction can be approximated using the following formula[13]:

$$k = (0.096 + 0.0033\text{MC} - 0.0008T)\cdot(0.105 + 2.03SG); \quad T < 0 \quad (\text{W/m/K})$$

$$k = (0.138 + 0.0019\text{MC} - 0.00022T + 0.000011\text{MC}\cdot T)\cdot(0.105 + 2.03\text{SG}); \quad T > 0 \quad (\text{W/m/K}) \quad (29)$$

SG is the specific gravity based on dry masse and green volume.

The independence of the thermal conductivity temperature is generally low; it is increases from 2% to 3% by 10°C.

Specific heat capacity

The specific heat capacity depends on both temperature and Moisture content; it is calculated by[13]:

$$C_{\text{p}} = 2280 + 16.6T; \quad T < 0 \quad (\text{J/kg/K})$$

$$C_{\text{p}} = 2000 + 8.71\text{MC} + 4.98T; \quad T > 0 \quad (\text{J/kg/K})$$

For wood thawing, the latent heat is determined by[13]:

$$L = L_{\text{w}}\left(\frac{\text{MC} - 30\%}{\text{MC} + 100\%}\right); \quad (\text{J/kg})$$

L_{w} is the latent heat of water fusion (334 kJ/kg).

For the finite element analysis, we consider a quadrilateral mesh with 1024 elements and 1089 nodes. The temperature history with phase change is given in Figure 3, showing computational and experimental data at the sample centre (eastern white pine).

During heating, when the wood was completely unfrozen and the log centre temperature approached the ambient temperature, the computational temperature increment was clearly smaller than the experimental temperature increment. In our opinion, this discrepancy may be related to incomplete experimental or numerical measuring (such convection losses to the outside). However, the numerical results show excellent agreement with the experimental data. In general, the discrepancy between measured and computed time is less than 5% for a given temperature.

APPLICATION

As an application, a prismatic 3D wood structure (trembling aspen) is considered; see Figure 4. The lower base of the structure is rectangular ($L_x = 2$ m by $L_y = 1$ m) with a height L_z that varies linearly from 0.1 to 0.025 meters in the radial direction. The microwaves are irradiated directly from the bottom of the

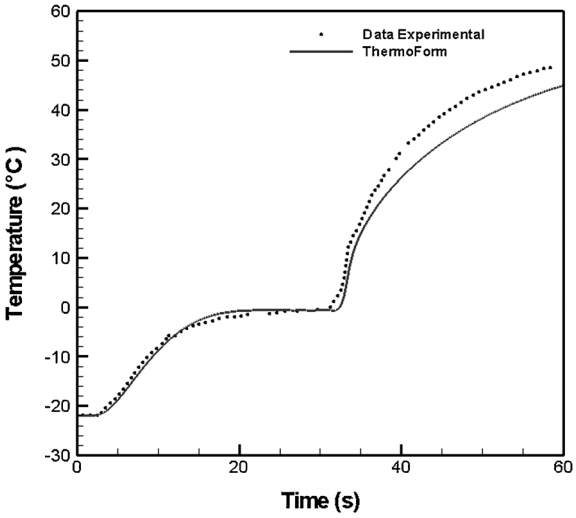

Figure 3. Change in temperature at the centre of the sample.

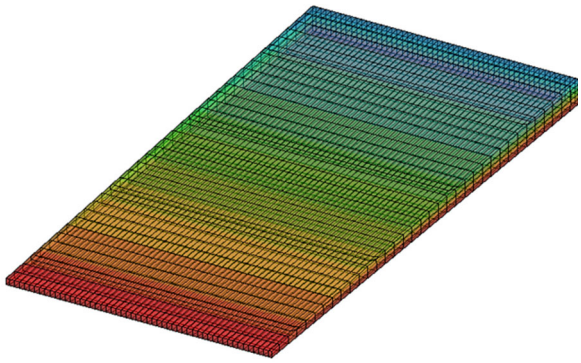

Figure 4. 3D geometry and mesh generation of for the sample.

rectangle upwards with an electric power of 2.01E4 (W). The initial temperature of the wood is −22°C and the heating time is fixed at 1000 s. For modelling with the 3D finite element method, the structure is meshed with identical hexahedra comprising eight nodes (5830 elements and 8154 nodes). For the analysis, we consider two frequencies (2466 and 912 MHz) and two moisture contents (57% and 115%). For the finite element analysis, we consider a hexahedral element mesh (3D) with 5830 elements and 8154 nodes (Figure 7).

Penetration Depth and Thermal Properties

The fundamental structure of wood, from the molecular to the cellular level, determines its properties and behaviour. The dielectric property reflects the wood's ability to absorb and store the material's electric potential energy when exposed to an electric field. This ability is described quantitatively by the dielectric constants, which depend on temperature and moisture content. It is generally accepted that for a given temperature, frequency and moisture content, the dielectric properties of wood do not change significantly with the electric field vector.[26] We therefore consider the generalised formulae given in Ref.[27] and applied to the species trembling aspen. Figures 5–7 illustrate the depth penetration profile for ($f = 2466$ MHz, MC = 57%), ($f = 2466$ MHz, MC = 115%) and ($f = 912$ MHz, MC = 115%), respectively.

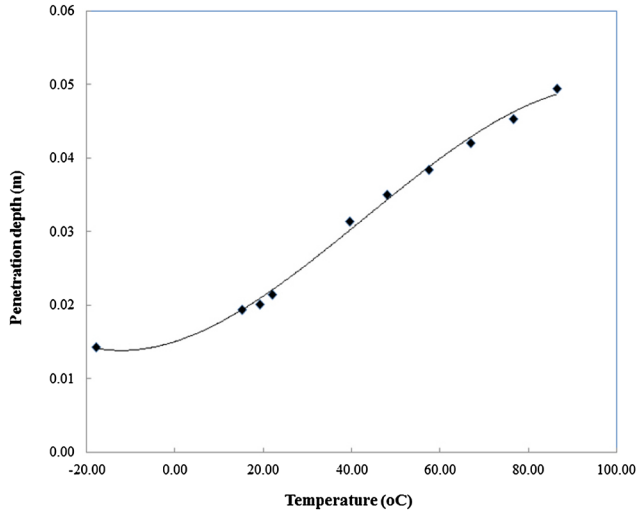

Figure 5. Penetration depth of penetration as a function of temperature (MC = 57% and $f = 2466$ MHz).

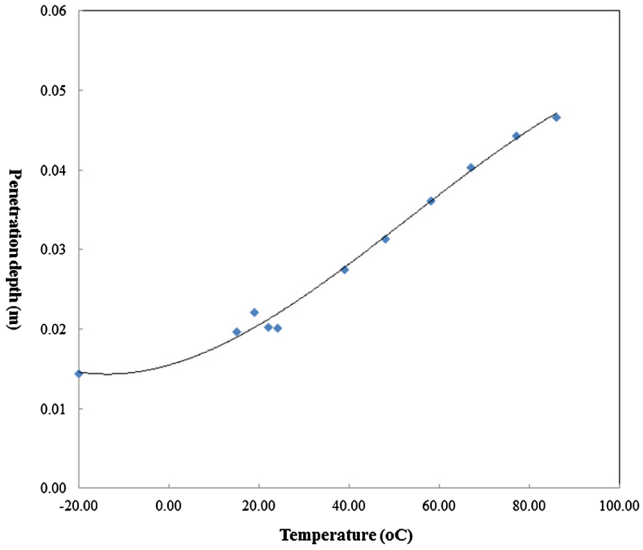

Figure 6. Penetration depth of penetration as a function of temperature (MC = 115% and $f = 2466$ MHz).

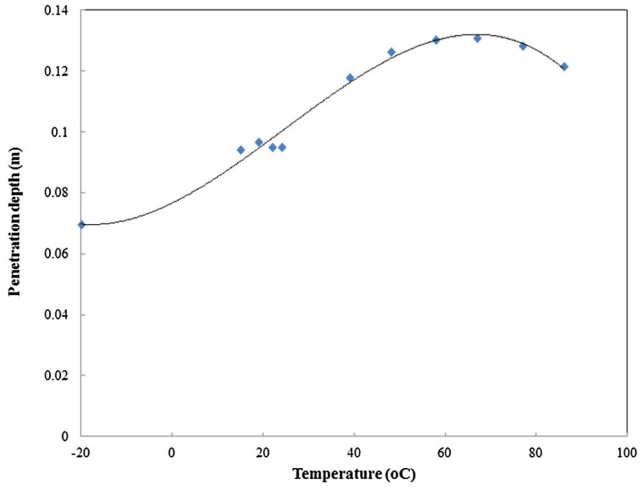

Figure 7. Penetration depth of penetration as a function of temperature (MC = 115% and $f = 912$ MHz).

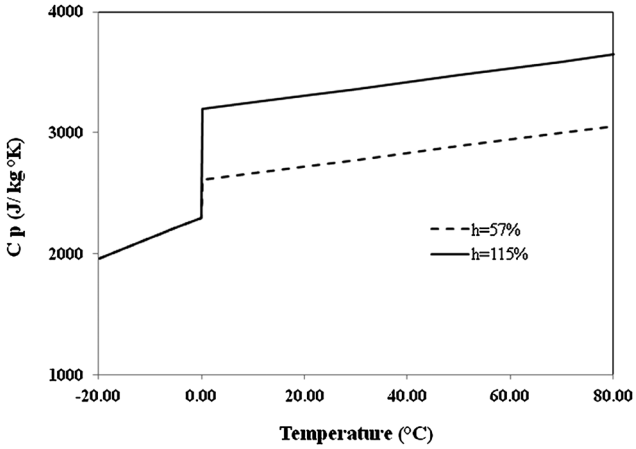

Figure 8. Heat capacity (J/kg K).

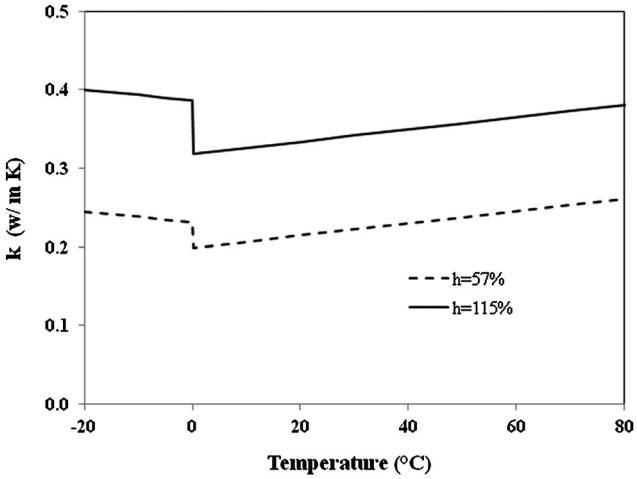

Figure 9. Thermal conductivity (W/m K).

The thermo-physical properties of the wood (specific heat capacity and the thermal conductivity for MC = 57% and MC = 115%) are given in Figures 8 and 9.[28] A typical value for trembling aspen density is 808.50 kg/m^3.

Results

Figures 10–11 illustrate the numerical results obtained for the temperature evolution, at different times throughout the center trace (x direction) and the thickness (z direction). In the Figure 10, for the frequency of 2466 MHz and at time $t = 1000$ s, on the face above the irradiated, and the respective positions ($x = 2$ m, $z = 0.12$ m) and ($x = 0$ m, $z = 1$ m), the temperature reached values of 90°C and 0°C. This temperature variation is explained by the position z (depending on thickness) of the two positions. However, at time $t = 250$ s, we see that the temperature is constant and independent of position x and z. This finding is explained by the accumulation of latent energy in the heating of the solid (ice presence) of the material. Once exceeded, the material temperature increases more easily. Same comment as for Figure 11 in z direction.

Figure 12 shows for the 2466 MHz frequency and a heating time of 1000 s, the effect of Moisture content on changes in temperature. We note that when the material is less humid it is more sensitive

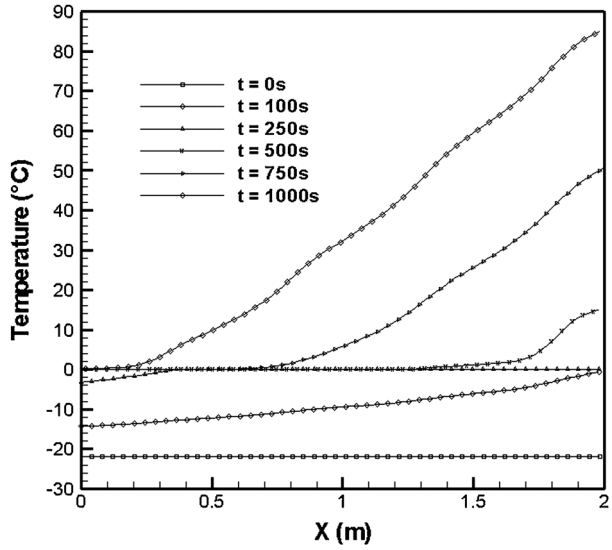

Figure 10. Temperature evolutions at different times throughout the centre trace.

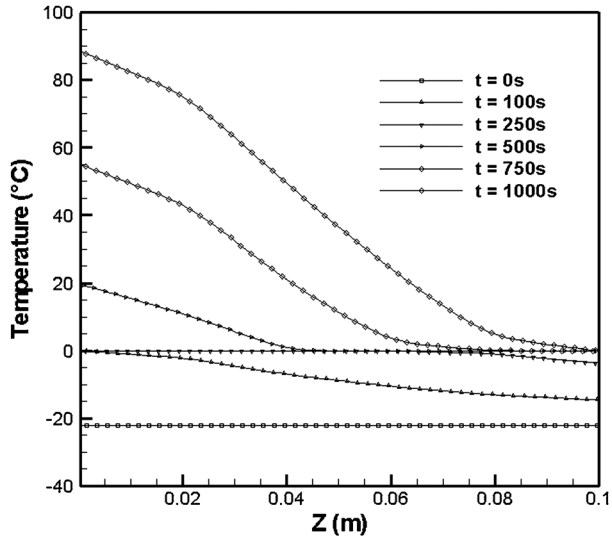

Figure 11. Temperature evolutions at different times throughout the thickness *h*.

to microwaves. Figure 13 shows for the 115% moisture content and a heating time of 1000 s, the effect of frequency (2466 MHz and 912 MHz) on the temperature evolution. The temperature of the material decreases with the frequency of the microwaves. This observation is consistent with the penetration depth expressions for frequencies 2466 MHz and 912 MHz (see Figures 6 and 7).

CONCLUSION

In this paper, the heating process of frozen wood exposed to plane microwaves is numerically investigated. The nonlinear heat conduction problem involving phase change such as wood freezing is solved by a specific 3D volumetric enthalpy-based finite element method. For the source term, a model of Beer–Lambert, arising from Maxwell's equations, was used. Dielectric and thermal properties are a function of temperature and moisture content. The numerical model is validated by experimental and analytical means. Finally an application is made on heating by microwave a strip of wood (*Trembling aspen type*).

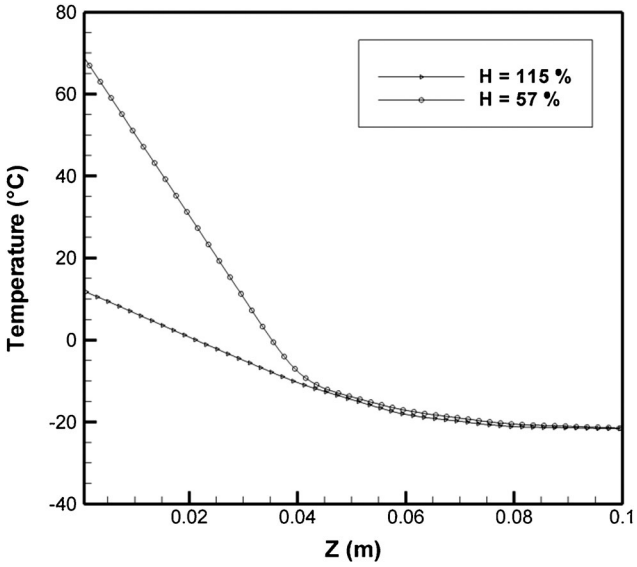

Figure 12. Effect of moisture content on the evolution of temperature ($f = 2466$ MHz).

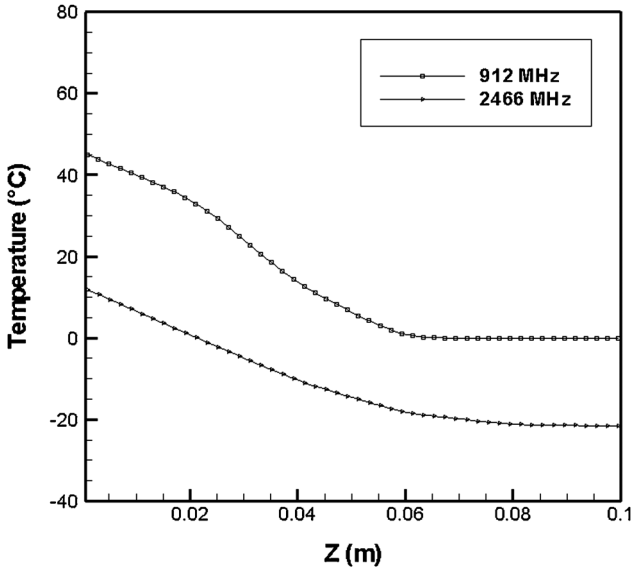

Figure 13. Effect of frequency on the evolution of temperature (MC = 115%).

ACKNOWLEDGEMENTS

We fully acknowledge the Natural Sciences and Engineering Research Council of Canada (NSERC) and the Fond de Recherche sur la Nature et les Technologies (FQRNT) for their financial support of this project.

REFERENCES

[1] R. Meredith, Engineers' Handbook of Industrial Microwave Heating, *IEE Power Series 25, Institution of Electrical Engineers*, London **1998**.

[2] E. Peterson, *Res. Chem. Intermediates* **1**994, *20*, 93.

[3] R. E. Mudgett, *Food Technol.* 1986, *6*, 84.

[4] E. J. Bond, X. Li, C. Hagness, B. D. Van Veen, *IEEE Trans. Antennas Propagation* **2**002, *51*, 1690.

[5] M. Chaplin, Water structure and Science. London South Bank University. Available at: www.lsbu.ac.uk/water/index.html. Accessed December 2004.

[6] G. Brodie, *Appl. Eng. Agric.* **2**007, *23*, 179.

[7] P. Rattanadecho, N. Suwannapum, *J. Heat Transf.* **2**009, *131*, 1.

[8] P. Rattanadecho, *Chem. Eng. Sci.* **2**006, *61*, 798.

[9] J. Zhu, A. V. Kuznetsov, K. P. Sandeep, *Int. J. Therm. Sci.* **2**007, *46*, 328.

[10] A. K. Datta, H. Prosetya, W. Hu, *J. Microw. Pow. Electromagn. Energy* **1**992, *27*, 38.

[11] T. Ohlsson, N. Bengston, *Microw. Energy Appl. Newsl.* **1**971, *6*, 3.

[12] S. Swami, Microwave heating characteristics of simulated high moisture foods. MS Thesis, University of Massachusetts, USA, 1982.

[13] H. Steinhagen, P. W. Harry, *Wood Fiber Sci.* **1**988, *20*, 451.

[14] A. A. Chen, R. K. Singh, K. Haghighi, P. E. Nelson, *J. Food Eng.* **1**993, *18*, 351.

[15] L. Zhou, V. M. Puri, R. C. Anantheswaran, G. Yeh, *J. Food Eng.* **1**995, *25*, 509.

[16] K. G. Ayappa, H. T. Davis, G. Crapiste, E. A. Davis, J. Gordan, *Chem. Eng. Sci.* **1**991, *46*, 1005.

[17] H. Ni, A. K. Datta, *J. Food Process Eng.* **2**002, *22*, 367.

[18] A. K. Datta, R. C. Anantheswaran, Handbook of Microwave Technology for Food Applications, Dekker, Inc., New York **2**001.

[19] H. Hu, S. A. Argyropoulos, *Model. Simul. Mater. Sci. Eng.* **1**995, *3*, 53.

[20] B. Nedjar, *Comput. Struct.* **2**002, *80*, 9.

[21] H. Flanders, *Am. Math. Mon.* **1**973, *80*, 615.

[22] K. A. Fikiin, *Int. J. Refrig.* **1**996, *19*, 132.

[23] M. A. Dokainish, K. Subbraj, *Comput. Struct.* **1**989, *32*, 1371.

[24] F. Erchiqui, I. Hamani, A. Charette, *Int. J. Therm. Sci.* **2**009, *48*, 73.

[25] W. Simpson, A. Tenwolde, Wood Handbook-Wood as an Engineering Material. Gen. Tech. Rep. FPL-GTR=113. Physical properties and moisture relations of wood. Chapter 3. U.S. Department of Agriculture, Forest Service, Forest Products Laboratory, Madison, WI **1999**.

[26] G. Torgovnikov, Dielectric Properties of Wood-Based Materials, Spinger-Verlag, Berlin **1**993.

[27] A. Koubaa, P. Perré, R. Hucheon, J. Lessard, *Drying Technol.* **2**008, *26*, 568.

[28] K. R. Kanter, *Derev. Prom.* **1**957, *6*, 17.

Manuscript received June 4, 2012; revised manuscript received August 29, 2012; accepted for publication August 29, 2012.